Utah State University
DigitalCommons@USU

Conference Proceedings | Materials Physics

6-30-2013

Nanodielectric Properties of High Conductivity Carbon-Loaded Polyimide Under Electron-Beam Irradiation

Amberly Evans Jensen
Utah State University

JR Dennison
Utah State Univesity

Justin Dekany
Utah State University

Gregory Wilson
Utah State University

Follow this and additional works at: http://digitalcommons.usu.edu/mp_conf

Recommended Citation
Amberly Evans Jensen, JR Dennison, Gregory Wilson, and Justin Dekany, "Nanodielectric Properties of High Conductivity Carbon-Loaded Polyimide Under Electron-Beam Irradiation," Proceedings of the 2013 IEEE International Conference on Solid Dielectrics (ICSD), (Bologna, Italy, June 30-July 4, 2013), pp.730-735. DOI: 10.1109/ICSD.2013.6619849

This Conference Paper is brought to you for free and open access by the Materials Physics at DigitalCommons@USU. It has been accepted for inclusion in Conference Proceedings by an authorized administrator of DigitalCommons@USU. For more information, please contact dylan.burns@usu.edu.

UtahStateUniversity
MERRILL-CAZIER LIBRARY

Nanodielectric Properties of High Conductivity Carbon-Loaded Polyimide Under Electron-Beam Irradiation

Amberly E Jensen, JR Dennison, Justin Dekany, and Gregory Wilson
Materials Physics Group, Physics Department, Utah State University
Logan, UT, USA
Amb.Eva@aggiemail.usu.edu, JR.Dennison@usu.edu

***Abstract*— Electron irradiation experiments were conducted to investigate the electron transport, charging, discharging, cathodoluminescence and emission properties of high-conductivity carbon-loaded polyimide (Black Kapton™). We discuss how these results are related to the nanoscale structure of the composite material. Measurements were conducted in an ultrahigh vacuum electron emission test chamber from <40 K to 290 K, using a monoenergetic beam with energies ranging from 3 keV to 25 keV and flux densities from 0.1 nA/cm^2 to 100 nA/cm^2 to deposit electrons in the material surface layer. Various experiments measured transport and displacement currents to a rear grounded electrode, absolute electron emission yields, electron-induced absolute photon emission yields and photon emission spectra (~250 nm to 1700 nm), and arcing rates and location. Numerous arcing events from the material edge to an electrically isolated grounded sample holder (particularly at lower temperatures) were observed, which are indicative of charge accumulation within the insulating regions of the material. Three types of light emission were also observed: (i) short duration (<1 s) arcing resulting from electrostatic discharge, (ii) long duration cathodoluminescence that turned on and off with the electron beam and (iii) intermediate duration (~100 s) glow that dissipated exponentially with time after infrequent and rapid onset. We discuss how the electron currents and arcing, as well as light emission absolute intensity and frequency, depend on electron beam energy, power, flux and temperature.**

Keywords—arcing, luminescence, conductivity, electron flux, low temperature, space environment interactions, materials testing, carbon composites

I. INTRODUCTION

High conductivity Black Kapton™ (HCBK) is a common nanodielectric composite material, with an insulating polyimide matrix that has been loaded with nanoscale turbostratic carbon particles to increase its electrical and thermal conductivity. On a macroscopic scale, HCBK acts as a good conductor, with conductivities ranging from 10^{-7} to 10^{-3} $(\Omega\text{-cm})^{-1}$ depending on the fraction of carbon-loading [1]. However, on the nanoscale the material exhibits both conducting and dielectric properties. The length scale is set by the size of the turbostratic carbon soot particles (~100-500 nm) and the carbon-depleted surface regions (~100-5000 nm depth) with separation of carbon-depleted regions (~3000-5000 nm) as shown in Fig. 1. This range of separation distances is comparable to the penetration depths of ~0.5-25 keV electrons into the composite of 800 to 11,000 nm [2].

Charging studies on polymers and carbon composites have revealed that sample arcing and luminescence occur as a result of electron beam bombardment [3-5]. Both insulating regions and electrically isolated carbon particles (floating conductors) can accumulate and dissipate charge; cathodoluminescence results from the insulating polyimide regions. These results have important consequences wherever Black Kapton™ is used in a charging environment—particularly at low temperature vacuum environments where charge dissipation is minimized—such as for spacecraft charging concerns in the space industry where HCBK use is ubiquitous. Arcing can damage the electrical components of a spacecraft causing malfunctions to occur [6]. Luminescence, if intense enough, could potentially produce optical contamination detrimental to the performance of the observatory optical elements and sensors, and act to limit their sensitivity and performance windows. As future space observatory missions push the envelope into more extreme environments and use more complex and sensitive detectors, a fundamental understanding of the dependencies of arcing and luminescent intensity on time, temperature, incident electron flux and energy, and material structure becomes critical.

II. EXPERIMENTATION

Electron beam experiments were conducted in the USU ultrahigh vacuum electron emission test chamber [7], modified for observations of low intensity UV/VIS/NIR glow over a broad range of sample temperatures [8]. A range of detectors is used with the system to measure a very broad range of temporal and spatial resolution, event durations, currents, energies, and electromagnetic wavelengths [9]. Fig. 2 provides a general schematic of the experimental system used [3, 4, 8, 10, 11].

A high-energy electron gun (Kimball, Model EGPS-21B)

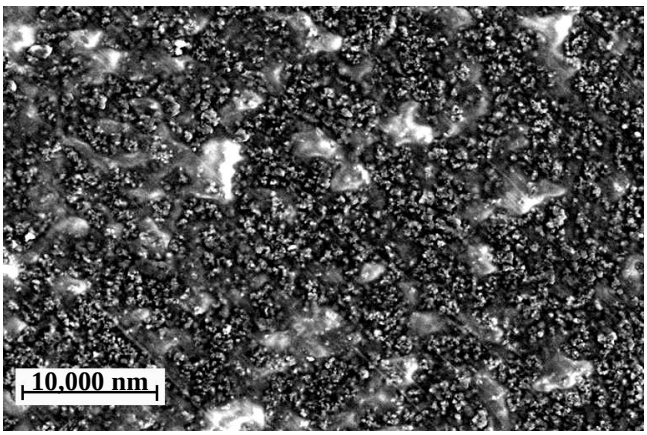

Fig. 1. Scanning electron micrograph of high conductivity carbon-loaded polyimide (Kapton™ 275XC230) showing ~0.1 um to 0.5 um diameter graphitic carbon black particles (darker areas) in a polyimide matrix with 1 um to 5 um diameter regions with no carbon particles near the surface (lighter areas). Image acquired at NASA Goddard Space Flight Center with an environmental SEM using a 5 kV beam.

Research was funded by the NASA Goddard Space Flight Center.

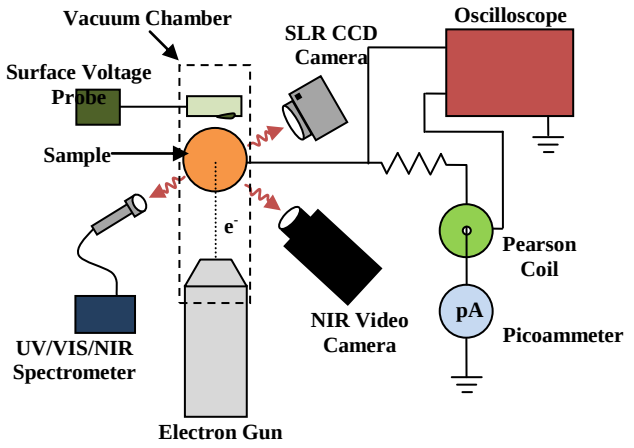

Fig. 2. Block diagram of instrumentation for collecting the pulse charging surface voltage, electrode current and cathodoluminescence data induced by electron beam bombardment. Instrumentation includes electrometers and a storage oscilloscope for current measurements and UV/VIS and IR spectrometers, an SLR CCD still camera, and CCD visible and NIR video camera for optical measurements.

provided incident electron energies of 5 keV to 25 keV with stable, uniform, well-characterized beam fluxes of 0.1 nA-cm^{-2} to 400 nA-cm^{-2} at typical beam spot diameters of ~3 cm [12]. The results discussed here are from tests at room temperature and 40 K, beam energies of 5, 7, 10, 15, 22 and 25 keV and beam current densities of 1, 10, 38 and 40 nA/cm^2. Absolute current densities were measured before and after each experiment with a conventional Faraday cup and relative fluxes were monitored in real time with a pseudo Faraday cup (B in Fig. 3a). Currents were measured from the back of the sample to ground, using fast sensitive picoammeters with <0.2 pA resolution [3]. A digital storage oscilloscope (Tektronix TDS 2040 1 GHz) acted as a shunt ammeter measuring the voltage drop across a 47 Ω metal-film resistor, typically with a 10^{-4} A threshold, 4 ns resolution, and 10 μJ sensitivity [9].

Three cameras and two fiber optic spectrometers were used to collect optical data [4, 9, 13] . Low light intensity was monitored with an SLR CCD still camera (Cannon, EOS Rebel XT DS126071; ~400 nm to 700 nm, 30 s/frame), a VIS/NIR image-intensified CCD video camera (Xybion, ISG-780-U-3; ~400 nm to 900 nm, 30 frames/s), and an InGaAs video camera (Goodrich Sensors Unlimited, SU320MS-1.7RT; ~800 nm to 1700 nm, 60 frames/s). UV/VIS (Stellarnet, 13LK-C-SR; ~200 nm to 1080 nm with ~ 1 nm resolution) and NIR (Stellarnet, RW-InGaAs-512; ~1000 nm to 1700 nm with ~ 3 nm resolution) spectrometers were also used. The spectral response and range were determined and the sensitivity of the instruments was calibrated with NIST traceable sources [8]. An additional InSb video camera, discreet detectors and filter combinations (~1000 nm to 5500 nm) were used to monitor IR emissions; no IR in the ~1100 nm to 2500 nm range was observed for any of the experiments reported here.

Two methods were used for sample cooling, a liquid N_2 cryogen reservoir (~150 K to ~400 K with a stability of ±4 K maintained over typical 2 hr experiment durations [14]) and a two-stage, closed-cycle helium cryostat (<30 K to >450 K, with long-term controlled stability of <0) [2].

The samples (10 mm diameter) of several grades of commercially available high conductivity Black Kapton™ material of increasing conductivity: Dupont 100XC10E5 [25 μm, $2\cdot10^{-5}$ (Ω-cm)$^{-1}$]; Dupont 100XC10E7 [25 μm, $3\cdot10^{-7}$ (Ω-cm)$^{-1}$]; Dupont 275XC230 [66 μm, $1\cdot10^{-3}$ (Ω-cm)$^{-1}$]; and a laminate composite with a Kevlar™ layer sandwiched between

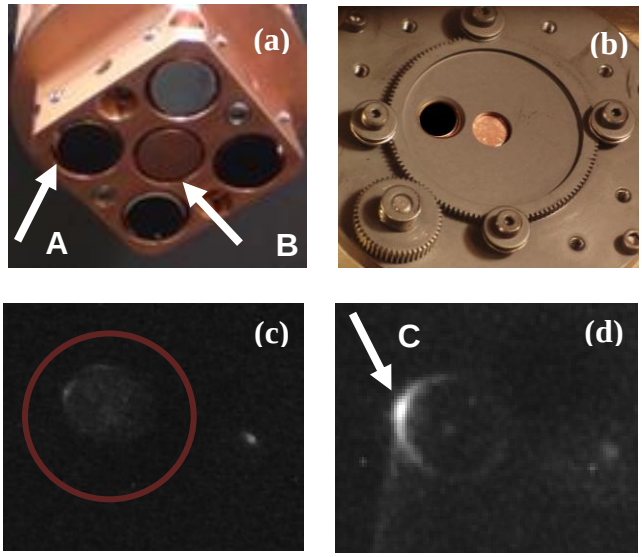

Fig. 3. (a) Sample mount with four samples **(A)** in the corners of the sample holder and a centered copper pseudo Faraday cup **(B)** for monitoring the beam current. **(b)** Rotating sample cover, which allows only the sample under investigation to be exposed to the beam. **(c)** Sample (in red circle), while the electron beam is on. (**d**) The position of an arc on the sample **(C)**.

two layers of two 275XC230 [254 μm, $5\cdot10^{-9}$ (Ω-cm)$^{-1}$], Dunmore 1100 Dun-Lam™ (thicknesses and room temperature conductivities across sample thickness measured at USU) [1]. At the low end of this temperature range, for Kapton™ the lower dark current conductivities [$2\cdot10^{-17}$ (rad-s^{-1})-(Ω-cm)$^{-1}$ at room temperature and $5\cdot10^{-18}$ (rad-s^{-1})-(Ω-cm)$^{-1}$ at 125 K] and radiation induced conductivities [$6\cdot10^{-20}$ (Ω-cm)$^{-1}$ at room temperature and $7\cdot10^{-21}$ (Ω-cm)$^{-1}$ at 125 K] led to reduced charge dissipation and enhanced charging and electrostatic discharges at low temperatures. The electrostatic breakdown field strength of Kapton™ at room temperature is $3\cdot10^{8}$ V-m^{-1} [15].

HCBK samples were optically cleaned and underwent a ~12 hr vacuum bakeout at ~390 K and <$1\cdot10^{-3}$ Pa to eliminate adsorbed water and volatile contaminates, and were placed in an ultrahigh vacuum chamber (base pressure <$1\cdot10^{-6}$ Pa) for > 24 hrs to allow for outgassing before measurements were made. The samples were mounted on Cu pedestals flush with an ~0.6 mm gap between the sample and a grounded multi-sample carousel (see Fig. 3(a)) [4].

III. Results

All types of Black Kapton™ samples studied exhibited readily observable electrical discharges and luminescence when subjected to electron beam bombardment, as illustrated in Fig. 4. Three types of light emission with simultaneous current signatures were observed: (i) short duration (<1 s) arcing resulting from electrostatic discharge, (ii) long-duration sustained glow (cathodoluminescence) that turned on and off with the electron beam, and (iii) intermediate duration (~10-100 s) glow that dissipated exponentially with time after infrequent and rapid onset. Arcs, sustained glow, and flares were all detected in the electrometer, oscilloscope, Vis SLR camera, Vis/NIR CCD video camera, and NIR InGaAs video camera; coincidence was almost always seen, except when the signals were below detection thresholds for specific instruments.

A. Arcs

HCBK exhibited numerous short duration (<1 s) electrostatic discharge or arcing events, as seen in Figs. 4 and

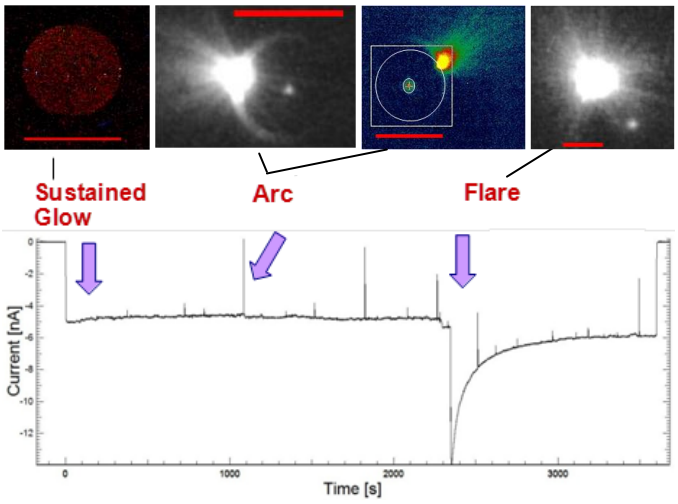

Fig. 4. Sample current of Black Kapton™/Kevlar™ composite (Dunmore 1100 Dun-Lam™) measured at 22 keV, ~500 nA/cm^2, and 144 K. A nearly constant current of ~5 nA associated with the sustained glow is observed from 0 s to 3600 s, while the beam is on. Large short-duration arcs are observed at ~1050 s, ~1820 s, ~2280 s, ~2490 s and ~2480 s; numerous smaller arcs are also evident. A large abrupt current spike at ~2345 s—with an approximately exponential decay with a ~50 s decay time—is labeled as a flare. The images above the graph, from left to right, are representative of similar optical signatures at 22 keV and 144 K: 30 s exposure SLR image at ~500 nA/cm^2; ~30 ms exposure CCD video image at ~5 nA/cm^2; ~16 ms exposure InGaAs video image at ~5 nA/cm^2; and ~30 ms exposure CCD video image at ~5 nA/cm^2. The rectangle, large circle, and small circle in the center image mark the regions for edge, sample and LaB_6 filament glow, respectively. The small LaB_6 filament spot is evident in the other images as well. The red bars are 10 mm scale bars.

5. Analysis of individual frames of camera data (see Fig. 4) allowed determination of the location of each arc, with a spatial resolution of <100 μm, as (almost exclusively) in the high electric field region in the gap between the sample edge and adjacent electrically isolated grounded sample holder. The time evolution of the average intensity in individual frames of camera data (after background subtraction from dark regions) was used to monitor behavior for three separate regions (sample surface, edge, and a weak glow from the light emanating from the LaB_6 filament of the electron gun at ~1700 K; refer to Fig. 4.). These intensity curves were larger for the edge regions, confirming the spatial locations of the arcs. The arcs spectral radiances are typically ~5-500X the intensities observed for sustained glow in the experiments reported here.

These current spikes from arcs, with typical ~0.5-5 nA amplitude and <1 nJ/arc, are evident in oscilloscope traces and in electrometer data for both the sample current and the sample holder (stage) current (see Fig. 4(a)). The increased negative currents observed in most (but not all) cases were indicative of rapid dissipation of accumulated electrons from within the insulating regions of the material to the grounded sample holder. There is not a clear correspondence between arc intensity in camera data and currents observed in the electrometer and oscilloscope data.

Fig. 6 shows the dependence from electrometer data of **(a)** number of arcs, **(b)** arc rate, and **(c)** average arc rate scaled by beam current density (or equivalently, number of arcs per deposited charge density) as a function of beam energy. Each of these displays an increase with increasing beam energy, although there are insufficient data with large error bars to determine if there are specific functional dependences for any of these cases. There is not a clear trend for the dependence of arc rate on incident current density.

Higher conductivity samples (275XC230 and 1100 Dun-Lam laminate) have similar arc rates and arc amplitudes/intensities for similar ranges of incident current, energy, power and temperature. Limited measurements at 22 keV and ~5 nA/cm^2 on lower conductivity (100XC10E7 and 100XC10E5) samples suggest that arc rates are ~2-10X higher than observed for higher conductivity (275XC230) samples at comparable energies and current densities.

Measurements were made from <40 K to 290 K. Lower temperature samples in general showed larger arc rates, although insufficient data have been acquired at different beam current densities and energies to establish a functional dependence. The dark current and radiation induced conductivities in polyimide are several orders of magnitude lower at the lower temperatures, leading to reduced charge dissipation and enhanced charging and electrostatic discharges at low temperatures.

Figs. 5 (b-e) show typical arc intensity curves as a function of time for electrometer, oscilloscope, CCD camera, and InGaAs camera measurements. Time constants for the exponential decays observed for many different arcs are fairly consistent for each individual instrument but vary substantially from instrument to instrument (electrometer: 10^0 s; CCD camera: 10^{-2} s; oscilloscope: 10^{-3} s; InGaAs camera: 10^{-1} s). In general, the oscilloscope data exhibit much faster response, with widths on the order of a few ms. The longer time constants exhibited in the other instruments are most likely the result of instrumental broadening. These response times longer than the arc duration cause the slower instruments to record a signal averaged over the slower response times; the different response times for different instruments makes cross-comparison of absolute peak amplitudes and power in the curves from different instruments difficult.

The generation of arcs in HCBK from incident electron flux at low temperatures and room temperatures and the approximate arc rates as reported here has been confirmed by limited measurements in independent studies [16, 17]. High frequency arc signatures, in radio frequencies, have also been observed with antennas near Black Kapton™ samples exposed to electron beams [18]. Additional investigations of how glow/arc/flare intensity, power and frequency scale with illuminated area are currently underway at USU and MSFC [16].

B. Sustained Glow

Sustained glow is long duration cathodoluminescence that turned on and off with the incident electron beam. It occurs over the full illuminated sample area when beam is on, as seen in Fig. 4. Fig. 5 shows that there is excellent temporal correlation between the electrometer data and the video camera spectral radiance curves. Sustained glow intensity or current takes a finite amount of time to reach a fairly steady equilibrium value. There is also a finite decay time seen in glow intensity and current curves after the beam is turned off. The exponential rise and decay time constants (10^{-1} s) are roughly the same and are believed to be related to filling and release rates of the traps in the insulating polyimide.

The magnitude of the sample currents during beam on times was consistent with a displacement current that resulted as charge accumulated in the sample. The rate of surface charging was typically close to the incident beam current density, J_b, reduced by the total electron yield of the sample at the incident beam landing energy, $d\Sigma/dt \propto J_b[1 - \sigma_{yield}(E_b, \Sigma)]$. At higher incident power levels, equilibrium

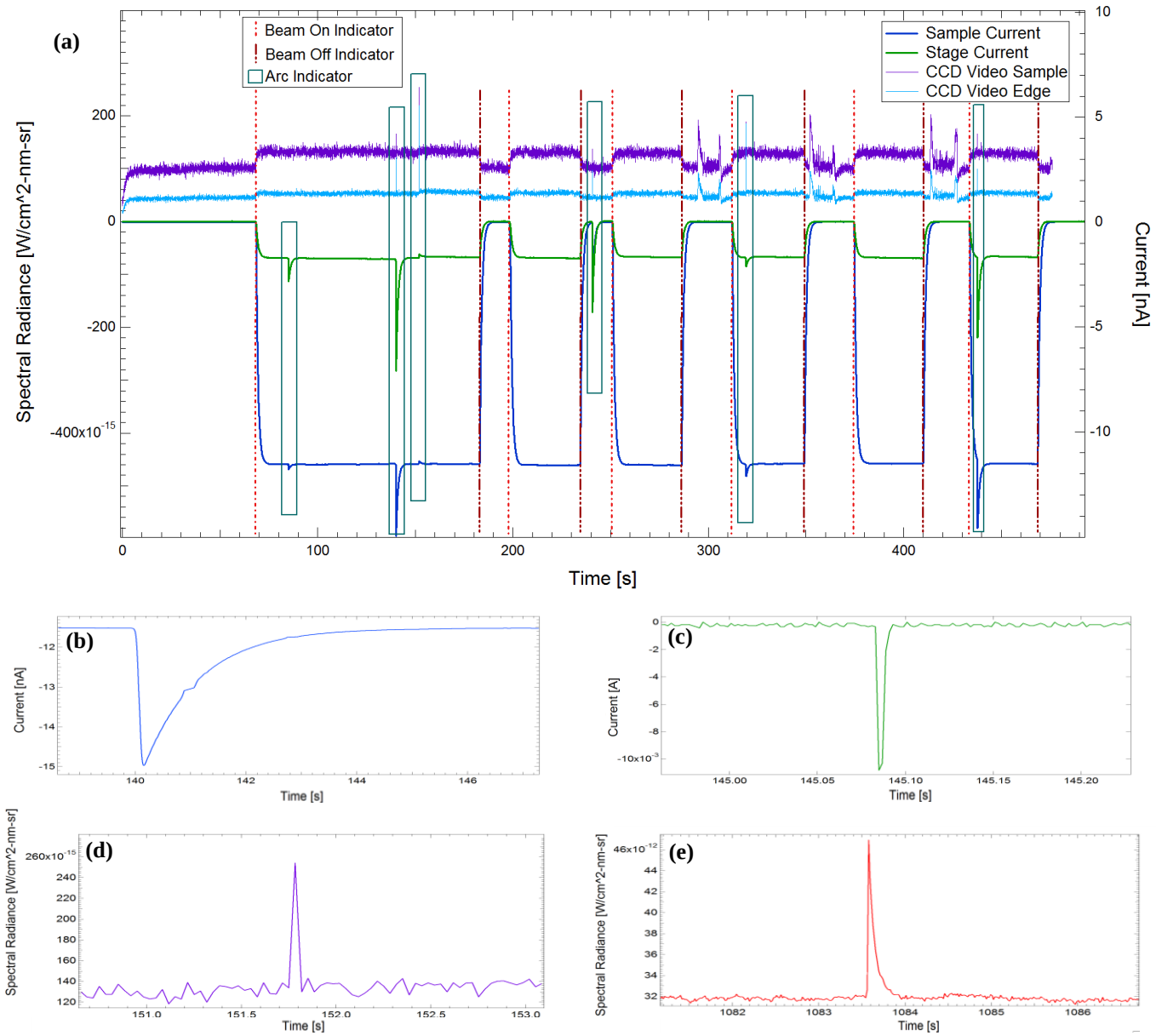

Fig. 5. (a) Absolute spectral radiance of the CCD visible video camera from the sample surface (purple curve) and edge (light blue) regions, respectively, plotted against elapsed time. Electrometer current data for the sample (dark blue curve) and stage (green curve), respectively, plotted against elapsed time. The times for electron beam-on (orange dotted vertical lines) and beam-off (brown dashed vertical lines); notice the corresponding changes in intensity and current. The noisy signals in the later three beam-off periods are due to extraneous external light sources. The sharp peaks enclosed in the turquoise boxes are identified as arcs; most arcs are seen in both the electrometer and video data. Typical arc signatures for: **(b)** electrometer; **(c)** oscilloscope; **(d)** CCD visible-range video camera; and **(e)** InGaAs NIR-range video camera.

glow intensity is sometimes seen to decrease ~2X due to long exposure of beam as the accumulated negative surface charge or reduced landing energy increased the electron yield, $\sigma_{yield}(E_b, \Sigma)$, toward unity.

Negative currents result from displacement currents to the grounded rear sample electrode and the grounded sample holder, as negative charge from the electron beam accumulates in the sample. Increased negative currents during arcs result from accumulated electrons in the sample moving to the grounded sample holder.

Simple models propose that luminescence increases linearly with incident power density (beam energy times beam current density) for non-penetrating radiation (*e.g.*, M55J carbon/epoxy composite data in Fig. 6(e)) and decreases in proportion to the range of incident electrons for penetrating radiation (*e.g.*, fused silica coating data in Fig. 6(e)) [13]. As seen in Fig. 6 (e), the spectral radiance of HCBK samples is largely independent of absorbed power. Bowers has proposed that a linear combination of thick polyimide regions (with non-penetrating radiation) and thin polyimide layers coating near-surface carbon particles (with penetrating radiation) can produce such a signature nearly independent of incident power [19]. The fraction of such regions can be approximated as the fraction of light (~36%) and dark (~64%) pixels in a binary image of the electron micrograph of Fig. 1 [20]. This simple luminescence model [13] for 10 nm (~0.4 keV penetration energy) and 50 µm (~60 keV penetration energy) in the ratio of thin to thick areas approximated by the SEM binary image [19] predicts the curve of spectral radiance versus energy shown in Fig. 6(e).

Higher conductivity samples (275XC230 and 1100 Dun-Lam laminate) have similar glow intensities for similar ranges of incident current, energy, power and temperature. Limited measurements at 22 keV and ~5 nA/cm2 on lower conductivity (100XC10E7 and 100XC10E5) samples suggest that sustained

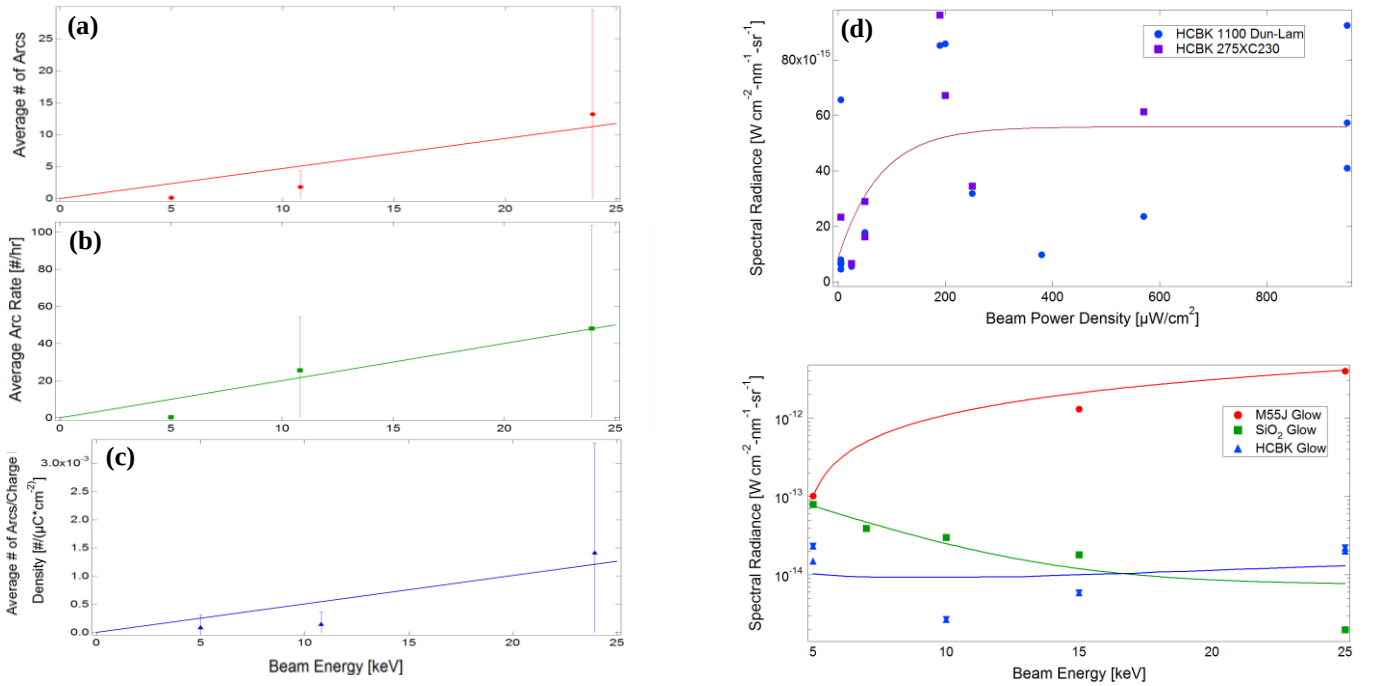

Fig. 6. Dependence of arcs and sustained glow on beam energy and power density. **(a)** Number of arcs, **(b)** arc rate, and **(c)** average number of arcs per deposited charge density, as functions of beam energy for low (5 keV), intermediate (7, 10 and 15 keV), and high (22 and 25 keV) energy beams with linear fits. **(d)** Spectral radiance versus beam power density of two types of HCBK materials (230XC275 and 1100 Dun-Lam™) based on a saturation curve [13]. **(e)** Total luminescent radiance versus beam energy at fixed 10 nA/cm^2 incident flux for: (red) epoxy-resin M55J carbon composite, shown with a linear fit for non-penetrating radiation; (green) SiO_2 coated mirror fit with decreasing intensity equation for penetrating radiation; (blue) carbon-loaded polyimide Black Kapton™ (triangles for 10 nA/cm^2 and hour glasses for 30 nA/cm^2 linearly scaled to 10 nA/cm^2), fit with a linear model for a linear combination of the penetrating and non-penetrating equations [13].

glow spectral radiance is ~2-10X lower than observed for higher conductivity (275XC230) samples at comparable energies and current densities. The amplitudes of the sustained glow increased roughly linearly with decreasing temperature and was approximately 8X brighter at 100 K than at room temperature.

Fig. 7 shows a low resolution plot of the sustained glow spectra that is peaked in visible near ~550 nm and extends into NIR. Calibrated measurements of the absolute spectral radiance with the cameras were consistent with the spectral measurements and were used to scale the spectra. This observed spectra is somewhat similar to cathodoluminescence of epoxy resin composites [5] and fused silica [13] observed previously.

C. *Flares*

Features seen simultaneously in current and VIS and NIR spectral response curves of intermediate duration (~100 s) glow that dissipated exponentially with time have been termed flares (see Fig. 4). Flares are infrequent (~2 flares/hr) and were only observed in long runs after ≥20 min duration, which suggests the necessity for substantial charging within the sample before flares can occur.

Flares (usually) have an arc associated with their instigation, although the origin of such large arc triggers is not known. Flares have abrupt onset rise times (<0.1 s), believed to be associate with a rapid discharge. Flares also exhibit very long times (10^2 s) for the currents or spectral radiance to return to pre-flare equilibrium values associated with sustained glow. The response for individual flares between the abrupt onset and long term decay is complex and can vary from one flare to the next.

The spectral response and electrometer currents ~1-100 nA amplitude with <1-10 μJ) of flares are ~2-20X that observed for typical sustained glow. Only about a half a dozen flares have been observed in ~20 hrs of HCBK data, too few to accurately determine the flare dependence on current density, charge fluence, beam energy, or deposited power. Flares seem to occur mostly for higher energies or power density; this suggests a possible link with charge dissipation through RIC. RIC allows lateral charge motion and downward motion in penetration region.

IV. Conclusions

High conductivity carbon-loaded polyimide underwent electron irradiation experiments to investigate the electron transport, charging, discharging, cathodoluminescence and emission behavior. These experiments revealed that for many applications HCBK cannot be viewed as a macroscopic conductor; it is a nanodielectric. This composite material is comprised of an insulating polyimide matrix with imbedded nanoscale conducting regions. Because the size of these regions is comparable to the length scales of electron penetration and transport, the material exhibits profound changes in the conducting and dielectric properties. Upon electron beam bombardment, the material exhibited behaviors similar to other dielectric materials; these include long duration cathodoluminescence, short duration arc and intermediate duration flare behaviors. As shown here, these properties can only be understood quantitatively by considering the nanoscale structure.

Acknowledgment

We gratefully acknowledge: contributions to instrumentation and experimental efforts from members of the Materials Physics Group (Ryan Hoffmann, Jerilyn Brunson, Jennifer Albretsen Roth and Jodie Corbridge Gillespie); help with optical calibrations from James Peterson of the USU Space Dynamics Laboratory; SEM measurements by Len Wang at NASA GSFC; use of the infrared and CCD video

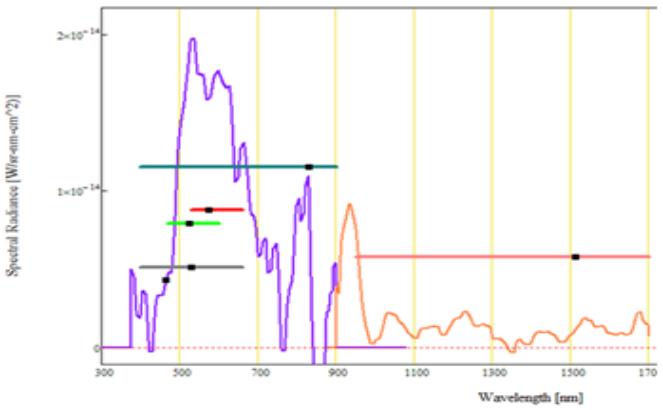

Fig. 7. Composite absolute spectral radiance of sustained glow from Black Kapton™/Kevlar™ composite (Dunmore 1100 Dun-Lam™) measured with UV/Vis (purple curve) and NIR (orange curve) spectrometers. Spectra amplitudes have been normalized to approximate the spectral radiance levels from the visible SLR camera (grey scale—grey bar, RGB—red/green/blue bars), visible/NIR video camera (turquoise bar), and NIR video camera (pink bar) where the heights of the bars show calibrated measurements of absolute spectral radiance, the lengths of bars show camera spectral ranges, and the symbols (■) indicate the camera weighted central wavelengths. Data were acquired at 22 keV, ~500 nA/cm^2, and 150 K. The spectral radiances have been scaled for a 7.3 µW/cm^2 incident electron beam at 22 keV.

cameras from Michael Taylor; and useful discussions with Charles Bowers, Robert Meloy, Malcolm Niedner and Jim Heaney of NASA GSFC, Todd Schneider of NASA MSFC, and Nelson Green of NASA JPL.

REFERENCES

[1] Dupont, "Technical data sheet: Dupont Dapton KC Black Anti-static Polyimide Film," *H-78314*, 2002.

[2] G. Wilson, and J.R. Dennison, "Approximation of range in materials as a function of incident electron energy," IEEE Trans. Plasma Sci., Vol. 40, 2012, pp. 291-297.

[3] A. Evans, G. Wilson, and J.R. Dennison, "Temperature dependence of SiO_2 electron-induced luminescence," Proc. Am. Phys. Soc. Four Corners Section Meeeting, Tucson, AZ, 2011.

[4] A. Evans, G. Wilson, J. Dekany, A.M. Sim and J.R. Dennison, "Low temperature cathodoluminescence of space observatory materials," Proc. 12th Intern. Spacecraft Charging Tech. Conf., Kitakyushu, Japan, 2012.

[5] V. Griseri, L. A. Dissado, J. C. Fothergill, C Laurent and G Teyssedre, "Photoluminescence, recombination induced luminescence and electroluminescence in epoxy resin," J. Phys. D: Appl. Phys., Vol. 34, 2001, pp. 2534–2540.

[6] R. Leach, and M. Alexander, "Failures and anomalies attributed to spacecraft charging," NASA Ref. Pub. 1375, Huntsville, AL: NASA Marshall Space Flight Center, 1995.

[7] W.Y. Chang, J.R. Dennison, N. Nickles and R.E. Davies, "Utah State University ground-based test facility for study of electronic properties of spacecraft materials," Proc. 6th Spacecraft Charging Tech. Conf., Hanscom Air Force Base, MA, 2000.

[8] J. Dekany, R.H. Johnson, G. Wilson, A. Evans and J.R. Dennison, "Ultrahigh vacuum cryostat system for extended low temperature space environment testing," Proc. 12th Intern. Spacecraft Charging Tech. Conf., Kitakyushu, Japan, 2012.

[9] J.A. Roth, R. Hoffmann, and J.R. Dennison, "Effects of radiation induced conductivity on electrostatic discharge in insulating materials," Proc. 1st AIAA Atmospheric and Space Environments Conf., San Antonio, TX, 2009, paper no. AIAA-2009-3527.

[10] G. Wilson, J.R. Dennison, A. Evans, and J. Dekany, "Electron energy dependent charging effects of multilayered dielectric materials," Proc. 12th Intern. Spacecraft Charging Tech. Conf., Kitakyushu, Japan, 2012.

[11] J. Hodges, J.R. Dennison, J. Dekany, G. Wilson, A. Evans, and A.M. Sim, "*In situ* surface voltage measurements of dielectrics under electron beam irradiation," Proc. 12th Intern. Spacecraft Charging Tech. Conf., Kitakyushu, Japan, 2012.

[12] G. Wilson, "The internal charge evolution of multilayered dielectrics undergoing mono-energetic electron bombardment," MS thesis, Utah State University, Logan, UT, 2013.

[13] J.R. Dennison, A. Evans, G. Wilson, J. Dekany, C.W. Bowers and R. Meloy, "Electron beam induced luminescence of SiO_2 optical coatings," Proc. IEEE Conf. Electr. Insul. Dielectr. Phen., Montreal, Canada, 2012.

[14] R. Hoffman, "Electron-induced yields of uncharged insulating materials," MS thesis, Utah State University, Logan, UT, 2010.

[15] J.C. Gillespie, "Measurements of the temperature dependence of radiation induced conductivity in polymeric dielectrics," MS thesis, Utah State University, Logan, UT, 2013.

[16] T. Schneider, NASA Marshall Space Flight Center, unpublished, 2013.

[17] N. Green, NASA Jet Propulsion Laboratory, unpublished, 2013.

[18] E. Wallach, NASA Goddard Space Flight Center, unpublished, 2012.

[19] C.W. Bowers, NASA Goddard Space Flight Center, unpublished, 2013.

[20] B.R. Jackson, X. Liu, E.F. McCandlish, and R.E. Riman, "Self-Assembly of Monolayer-Thick Alumina Particle-Epoxy Composite Films," Langmuir, Vol. 23, 2007. pp. 11399-11403.

.